Exciton Delocalization in the B850 Light-Harvesting Complex: Comparison of Different Measures

M. Dahlbom,[†] T. Pullerits,[†] S. Mukamel,*[,‡] and V. Sundström*[,†]

Department of Chemical Physics, Lund University, Box 124, 211 00 Lund, Sweden, and Department of Chemistry, University of Rochester, Rochester, New York 14627

Received: December 14, 2000; In Final Form: March 19, 2001

A much debated topic in recent studies of ultrafast exciton dynamics in molecular aggregates has been the precise definition of the exciton coherence domain in the B850 aggregate of photosynthetic purple bacteria. In this work we compare several measures of exciton delocalization and their variation with temperature, inhomogeneous broadening, and time. We find that the exciton wave packet prepared by a 40 fs pulse is initially delocalized over a substantial portion of the ring and contracts to a significantly smaller size on the time scale of a few hundreds of femtoseconds. Steady-state absorption and time-dependent pump−probe spectra of the B850 aggregate are simulated and compare well with previously reported experimental data. The calculated thermalized exciton wave packet size is in good agreement with previous experimental and theoretical estimates.

I. Introduction

Molecular aggregates belong to a family of molecular nanostructures that lies between crystals and isolated molecules. J-aggregates,[1] polymers,[2] photosynthetic antenna complexes,[3] and dendrimers[4,5] are a few examples of such systems. As the number of chromophores in the aggregate (N) is increased, the system properties change from molecular to bulk type, and size-dependent effects must be considered in aggregates, including energy transfer, resonance interaction, exchange narrowing, and collective spontaneous emission (superradiance). Collective excited states, excitons, are formed in molecular crystals and aggregates due to strong coupling.[6,7] In an ideal system, without exciton−phonon interactions and static disorder, the molecular exciton states would be perfectly delocalized over the entire aggregate. However, various perturbations may localize these states to a part of the aggregate. There are a number of localization mechanisms to consider: static (on-site energetic and orientation) disorder, exciton−phonon coupling (dynamic disorder and polaron formation) and impurities. In one-dimensional molecular aggregates the delocalization of the exciton can be well described by a length scale, L_d, i.e., the number of molecules that share the excitation. In general, however, higher dimensionalities or fractal structures necessitate a broader definition of an exciton delocalization domain (ECD).[8,9]

The ECD of Frenkel excitons lends itself to a simple real space visualization, enabling intuitive interpretation of excitation dynamics and a deeper understanding of how interaction strength and homogeneous and inhomogeneous broadening contribute to the spectroscopic properties of the molecular aggregate.

Photosynthetic antenna systems have been used as prototypes for studies of exciton effects.[10] Recently, the structure of the peripheral light-harvesting complex (LH2) of photosynthetic purple bacteria was determined to atomic resolution for *Rhodopseudomonas (Rps.) acidophila*[11] and *Rhodospirillium molischianum*.[12] LH2 contains two concentric rings of bacteriochlorophyll (BChl) molecules named B800 and B850 after their characteristic Q_y absorption maxima at 800 and 850 nm (see Figure 1). Surrounding the BChl pigments is a cylindrical "cage" formed by α and β protein helicies. In *Rps. acidophila*, the B800 ring consists of 9 well-separated BChl molecules, roughly 18 Å apart, with excited states having a localized character.[13] Contrary to that, the 18 BChl molecules of the B850 ring are densely packed with center-to-center distances of about 9 Å, and strong intermolecular interaction leads to a considerable delocalization of the excitations. Various experimental and theoretical techniques have been employed to characterize the exciton,[14−33] and the resulting values of L_d range from a few pigment molecules[15−19] to the entire ring.[31,32] In this paper we will show that the large variation in L_d obtained by different authors is the result of different definitions of the exciton delocalization, as well as different experimental probes for exciton coherence.

Localization properties of individual exciton eigenstates can be defined and analyzed. However, in most experiments the signals depend on superpositions of many such eigenstates, making it impossible to connect the individual eigenstates directly with observables. Mukamel and co-workers have developed descriptions of optical signals of chromophore aggregates based on the excitonic density matrix N_{mn} (eq 2.6).[34−36] These include nonlinear susceptibilities (frequency domain)[34,35] as well as pump−probe, fluorescence, and cooperative spontaneous emission (superradiance).[14,15,21,36−39] An electron−hole density matrix has been also used to measure the coherence size in conjugated polymers.[2,4,40] The diagonal elements of the density matrix N_{nn} (in the real space, chromophore, representation) give the populations of the various chromophores. However, more interesting is to look at the antidiagonal directions, i.e., the variation of N_{mn} with $n - m$.[35,36] The density matrix is the most natural way of characterizing the coherence size, and the exciton density matrix provides a

[†] Lund University.
[‡] University of Rochester.

10.1021/jp004496i CCC: $20.00
Published on Web 05/18/2001

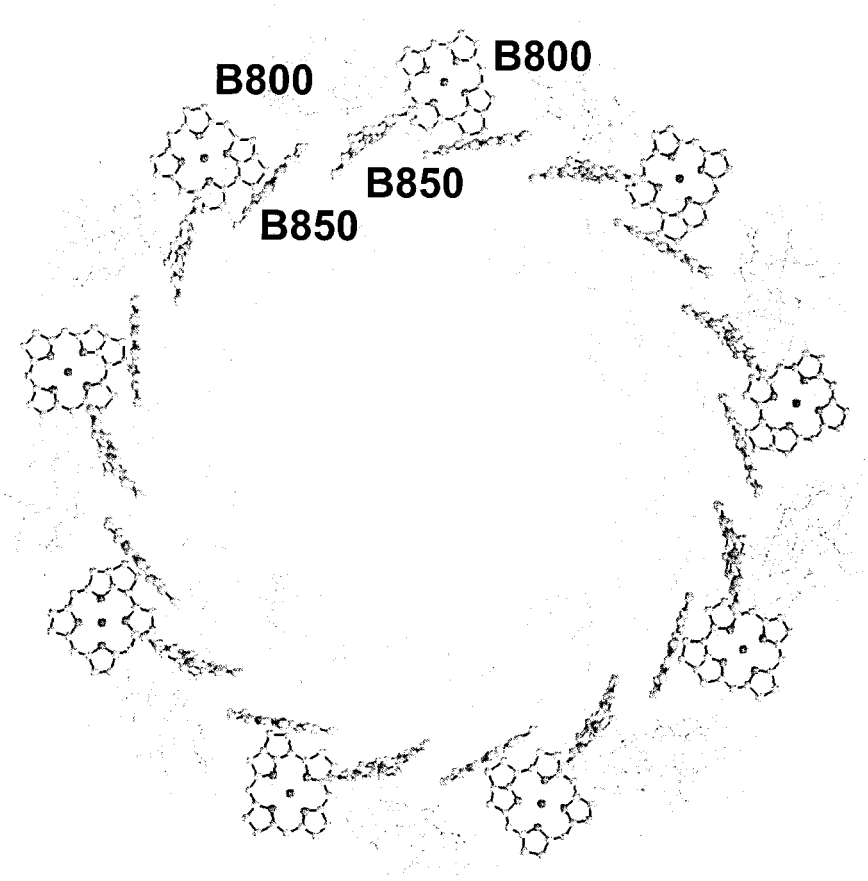

Figure 1. Two concentric BChl rings in the LH2 complex of *Rps. acidophila* seen in their protein environment. The pigments parallel to the surface belong to B800 and the perpendicular to B850.[11]

direct measure of exciton coherence that is closely connected to experimental signals such as pump−probe[15,21] and cooperative spontaneous emission superradiance.[41] It is reasonable to assume that the initial exciton wave packet created by a femtosecond pulse is delocalized over a substantial part of the ring and through the mechanisms described earlier it rapidly becomes localized on a smaller set of chromophores.[15,20,42]

In this paper we simulate the time dependent localization of the B850 exciton as reflected in experimental transient absorption and superradiance measurements. We further compare several definitions of L_d and examine their differences. The article is organized as follows: In section II, we present the Frenkel exciton model for the aggregate and express the pump−probe spectroscopy and superradiance in terms of the exciton density matrix. The various definitions of L_d are given and discussed in section III. Numerical calculations are presented in section IV, and the conclusions are drawn in section V.

II. The Exciton Density Matrix in Pump−Probe Spectroscopy and Superradiance Experiments

In this section we briefly review the model that describes the B850 aggregate as a set of coupled three-level systems. We discuss the real space doorway−window formulation of ultrafast pump−probe spectroscopy and superradiance. The time-dependent exciton density matrix will be used to calculate the different exciton delocalization length estimates defined in the following section.[14,43]

The B850 aggregate has a 9-fold ring symmetry consisting of 18 weakly dimerized BChl(a) molecules (Figure 1). The model chromophores have a ground state (S_0), a first excited state (S_1), and a second excited state (S_2). The ground-state absorption spectrum corresponds to the $S_0 \rightarrow S_1$ transition, the so-called Q_y transition. In our calculations we use a Green function formulation of the optical response functions in the real-space doorway−window representation.[14,44] The calculation can be divided into three steps: First, (i) the pump pulse excites an exciton wave packet, the doorway, in the system. During the pulse delay this initial wave packet then interacts with the surrounding environment (step ii). Finally, (step iii) the probe pulse creates a second wave packet, the window, and the Liouville space overlap with the propagated doorway wave packet results in the pump−probe signal. The doorway−window expressions use the Wigner spectrogram representation of the fields.[44,50,51] This mixed time and frequency representation is well suited for the spectroscopic simulations performed in this paper since pulses of arbitrary shapes and durations can be used.

The electronic motions are described by the Frenkel Hamiltonian, which in the Heitler−London approximation reads,[45]

$$H = \sum_{mn} h_{mn} \hat{B}_m^\dagger \hat{B}_n + \sum_n \frac{g_n}{2} (\hat{B}_n^\dagger)^2 (\hat{B}_n)^2 - E(t)\cdot P \qquad (2.1)$$

$\hat{B}_m^\dagger$ ($\hat{B}_m$) are the exciton creation (annihilation) operators that create (remove) an excitation on the mth chromophore, satisfying the commutator relations

$$[\hat{B}_n, \hat{B}_m^\dagger] = \delta_{mn}(1 - (2 - \kappa_n^2)\hat{B}_n^\dagger \hat{B}_n) \qquad (2.2)$$

The Hamiltonian matrix elements are $h_{mn} = (E_n\delta_{mn} + J_{mn})$ and $g_n \equiv 2\hbar((2 - \kappa_n^2)\Omega_n + \Delta_n)/\kappa_n^2$ is the nonlinearity parameter. The energetic offset of the chromophores from a harmonic three-level structure is measured by Δ_n so that the energy gap between the S_2 and S_1 levels is $(\Omega_n^{(2)} - \Omega_n^{(1)} = (\Omega_n + \Delta_n)$. g_n contain all the information about the two-exciton state manifold and thus we can avoid explicit calculation of this manifold. κ_n is the ratio of the $S_1 \rightarrow S_2$ and $S_0 \rightarrow S_1$ transition dipoles of the individual chromophores.[45] The polarization operator, which controls the interaction term between the system and the external field, $E(t)$ reads

$$P = \sum_n \mu_n(\hat{B}_n^\dagger + \hat{B}_n) \tag{2.3}$$

We further assume that the electronic system is linearly coupled to a bath of harmonic oscillators representing the surrounding environment. The collective coordinates of the nuclear oscillators are eliminated using projection operator techniques,[46] and the bath influence on the electronic system is completely contained in the Redfield relaxation superoperator.[46−49]

The one-exciton energies and wavevectors can be obtained from the eigenrelation $\sum_n h_{mn}\varphi_\alpha(n) = \epsilon_\alpha\varphi_\alpha(m)$ and the transition dipole in the exciton representation is then $\mu_\alpha = \sum_m \varphi_\alpha(m)\mu_m$. Using the exciton basis, the linear absorption spectrum is given by[14]

$$S_{abs}(\omega) = \sum_\alpha \frac{2|\mu_\alpha|^2\epsilon_\alpha}{(\omega - \epsilon_\alpha)^2 + \Gamma^2} \tag{2.4}$$

where Γ is a phenomenological electronic dephasing rate, corresponding to the half-width at half-maxima of the Lorentzian line-shape function.

The pump−probe signal in the doorway−window representation was calculated by solving the nonlinear exciton equations (NEE),[45]

$$S_{pp}(\tau,\bar{\omega}_2,\bar{\omega}_1) = \sum_{mn}\int_0^\infty d\tau' \int_0^\infty dt_2\, W_{mn}(\tau-\tau',\bar{\omega}_2)\, N_{mn}(\tau'-t_2,\bar{\omega}_1) \tag{2.5}$$

The exciton density matrix (EDM), is defined as

$$N_{mn}(t) = \langle \hat{B}_m^\dagger(t)\, \hat{B}_n(t)\rangle \tag{2.6}$$

Following the interaction with the pump, the time-dependent exciton density matrix can be represented by the propagated doorway function defined as

$$N_{mn}(\tau'-t_2,\bar{\omega}_1) \equiv \sum_{kl} \bar{G}_{mn,kl}(t_2)\, D_{kl}(\tau'-t_2,\bar{\omega}_1) \tag{2.7}$$

where the initial exciton density matrix is given by the doorway function. Expressions for the doorway (D) and window functions (W), dressed with the Wigner spectrograms of the pulses,[50,51] are given in ref 44. The time arguments τ, τ', and t_2 are related to the time delay between the pump and the probe pulses, and the overall pulse characteristics, whereas $\bar{\omega}_1$ and $\bar{\omega}_2$ are the central frequencies of the pump and probe pulses. The superoperator $\bar{G}(t)$ represents the evolution of the exciton density matrix. It incorporates the phonon bath influence on the system using the Redfield relaxation superoperator.[48,49,52] Each molecule is coupled to an uncorrelated-oscillator bath, which is modeled using the spectral density of the overdamped Brownian oscillator;[14,46] see ref 44 for details.

Another observable, the superradiance enhancement factor, which represents the radiative decay rate of the aggregate relative to that of the monomer, is given by[15]

$$L_s(\tau) = \sum_{mn} M_{mn}N_{mn}(\tau) \tag{2.8}$$

The window function is given by $M_{mn} = \mathbf{d}_m\cdot\mathbf{d}_n$ and contains all the relevant geometric information about the system. Here $\mathbf{d}_n$ is the unit dipole vector of the nth chromophore. Superradiance offers perhaps the most direct connection between an experimental observable and the EDM. When all dipoles are parallel (a linear aggregate), $M_{mn} = 1$, and L_s provides a direct estimate of the exciton delocalization length. Otherwise L_s shows an interplay of geometry and exciton dynamics. Thus, the superradiance factor of a ring structure like B850 does not give a direct measure of the exciton size. An observed L_s can be the result of the delocalization length L_s or $N_0 - L_s$, where N_0 is the system size. This means that small L_s may imply either a highly localized or delocalized exciton. Additional measurements like the temperature dependence of L_s[18] or single molecule spectroscopy[24] can resolve this ambiguity.

III. Measures of the Exciton Delocalization Length

The extent of delocalization of the optically generated exciton wave packet strongly influences the signals obtained in various optical measurements, and in order to fully understand the light-harvesting energy transfer mechanisms, it is important to characterize the properties of the basic excitations. Experimentally, L_d has been estimated from pump−probe spectra peak-splitting[17] (the energetic difference between the excited-state absorption and the ground-state bleaching peaks), the absorbing dipole strength,[25,32,54] and superradiance measurements.[18,53−55] Theoretically, several tools have been proposed and used to estimate this property.[15,16,23,29] Different authors have reported L_d values ranging from a few pigment molecules[15−19] up to the full ring.[31,32] Some of this discrepancy may be attributed to the use of different definitions. However, more importantly, different experimental techniques are expected to yield different coherence sizes. For instance, time-resolved and steady-state methods should give different results if the exciton delocalization length is time dependent. The exciton wave functions are linear combinations of molecular states, since electronic coupling causes molecules to behave coherently. The coherence can be reduced by static and dynamic disorder, which leads to localization. On the other hand, a short and spectrally broad excitation pulse creates a coherent superposition of a number of exciton states, i.e., an excitonic wave packet. Because of interference, the wave packet may have a major part of its amplitude in a very localized region of the aggregate.[56] The coherence between exciton levels is rapidly destroyed due to dephasing and exciton relaxation. In some sense this can be seen as if an initially localized wave packet is delocalized by dephasing processes. However, we should keep in mind that the initially prepared excitonic wave packet (doorway state) may seem localized even if it has a precise phase-relationship between different molecular states over the entire aggregate. This illustrates the possible difficulties in discussing the interplay of coherence and localization.

A number of different definitions have been used for characterizing the exciton delocalization length. We reserve L_d for the generic exciton delocalization length and denote specific measures by different subscripts. Meier, Chernyak and Mukamel[15] considered the entire $|N_{mn}(t)|$ (both diagonal and off-diagonal elements) as a distribution. The exciton delocalization

length, was then defined as the inverse participation ratio associated with this distribution

$$L_\rho(t) = [N_0 \sum_{mn} |N_{mn}(t)|^2]^{-1} [(\sum_{mn} |N_{mn}(t)|)^2] \qquad (3.1)$$

In this expression, N_0 is the system size and the EDM is defined in eq 2.7. L_ρ is a length scale on which the EDM decays along the anti-diagonal direction, and an intuitive measure that connects directly with experimental measurements.

Kühn and Sundström[23] defined the exciton delocalization length (L_{ks}) as the full width half-maximum (fwhm) of the distribution function

$$C_n(t) \equiv \sum_m |\langle N_{m,m+n}(t) \rangle_{\text{disorder}}| \qquad (3.2)$$

This measures an autocorrelation distribution for site n of the exciton density matrix, averaged over the coherence contributions from all other sites in the aggregate. L_{ks} is obtained by calculating the distribution from $n = 0$ to 8 (for B850 of LH2) and taking the fwhm of this distribution. If the excitation is completely localized at one site (e.g., site 0), the distribution will be 1 at site 0 and exactly 0 for sites 1−8, but if the excitation is more delocalized, the distribution will be broader according to the extent of coherence between the pigments. Furthermore, all one-exciton wave functions except for the lowest and highest (usually denoted $k = 0$ and 9) are oscillatory and therefore the fwhm estimate will be increasingly difficult to obtain with increasing exciton delocalization. If the coherence between the exciton levels is dephased, this definition corresponds exactly to the autocorrelation definition used in refs 18 and 30.

The participation ratio is based on general properties of distribution functions. The localization characteristics of a disordered system can be described using a set of functions based on the sum over the density distribution of the wave function[57−60]

$$I_n = \sum_i |\varphi_i|^{2n} \qquad (3.3)$$

where φ_i is the wave function for the ith exciton level for a one-dimensional discrete lattice. This quantity may be averaged over the Boltzmann distribution of exciton states

$$I_n = \sum_i \left(\frac{P_i}{Z}\right) |\varphi_i|^{2n} \qquad (3.4)$$

$I_1 = 1$ whereas $1/I_2$, known as the inverse participation ratio, is a measure of the width of the distribution and can be used as an estimate of the exciton delocalization length.

Leegwater[16] defined the exciton delocalization length as a generalized inverse participation ratio

$$L_{gr}^{-1} = \sum_{i,\alpha,\alpha'} |\langle i|\varphi_\alpha\rangle|^2 \sqrt{\frac{P_\alpha}{Z}} \frac{\Gamma^2}{\Gamma^2 + (\omega_\alpha - \omega_{\alpha'})^2} |\langle i|\varphi_{\alpha'}\rangle|^2 \sqrt{\frac{P_{\alpha'}}{Z}} \qquad (3.5)$$

where φ_α is the exciton wave function and Γ is the exciton dephasing rate. $P_\alpha = \exp(-\epsilon_\alpha/k_BT)$ is the Boltzmann factor of state α and $Z = \sum_\alpha \exp(-\epsilon_\alpha/k_BT)$ is the canonical partition function where k_B is the Boltzmann constant.

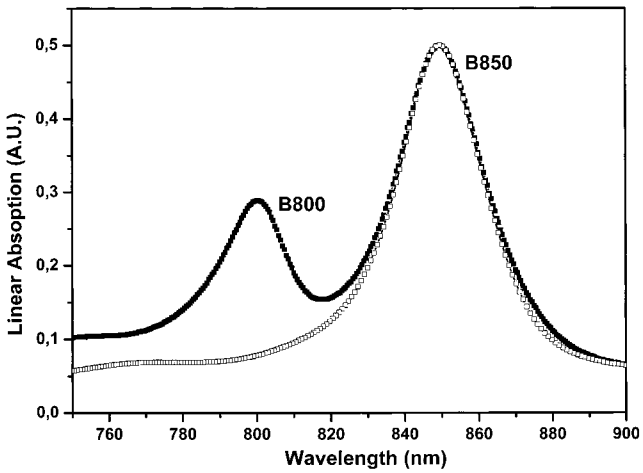

Figure 2. Linear absorption spectra of LH2 from *Rps. acidophila* at room temperature: (open circles) experimentally recorded; (filled squares) simulated absorption spectra for an inhomogeneous broadening of 250 cm^{-1}, a homogeneous line width of 75 cm^{-1}, and the first excited molecular state at 12 426 cm^{-1}.

The ordinary inverse participation ratio,[29] a special case of L_{gr}, has been extensively used for light-harvesting systems.[20,26,30] By setting $\Gamma = 0$, eq 3.5 yields

$$L_{ipr}^{-1} = \sum_{i,\alpha} |\langle i|\varphi_\alpha\rangle|^4 \frac{P_\alpha}{Z} \qquad (3.6)$$

It is straightforward to add time dependence to the definitions of L_{gr} and L_{ipr} by including the population dynamics of the exciton states ($P_\alpha(t)$). However, inter-exciton-level coherence and dephasing are not accounted for in these two definitions.

IV. Application to the B850 System

We describe the B850 antenna by a model aggregate made out of 18 three-level systems with dipole−dipole coupling. Existing literature does not provide unique values for the characteristics of these systems. A wide range of interaction strengths has been proposed for the B850 aggregate, ranging from 200 up to 800 cm^{-1}. Accumulating evidence suggests a nearest neighbor interaction of about 300 cm^{-1}; for a review see ref 30. We have estimated the interaction energies using the structure of *Rps. acidophila* and assuming dipole−dipole interaction. The B850 aggregate consists of a slightly dimerized ring-structure where the nearest neighbor interactions alternate between $J = 340$ and 230 cm^{-1}. All other pairwise interaction terms are included, but they are all less or equal to 46 cm^{-1}. The disorder was drawn from a Gaussian distribution function

$$P(\epsilon_n) = \frac{1}{\sigma\sqrt{2\pi}} \exp(-\epsilon_n^2/2\sigma^2) \qquad (4.1)$$

where the distribution of ϵ_n represent the uncorrelated static fluctuations of the energy levels caused by the surrounding protein cage, and σ is the variance of this distribution. We used a width (σ_{inh}) of the inhomogeneous broadening (energetic disorder) of 255 cm^{-1} (variance); see Figure 2. This disorder is in agreement with values used in other recent works.[15,18,30] The homogeneous (the inverse of dephasing constant), $\Gamma = 75$ cm^{-1}, and the transition energy for the first excited molecular state ($S_0 \rightarrow S_1$), $E_i = 12\,426$ cm^{-1}, were estimated by comparing the calculated linear and transient absorption spectra with the experimental room-temperature spectra. The assignment of the

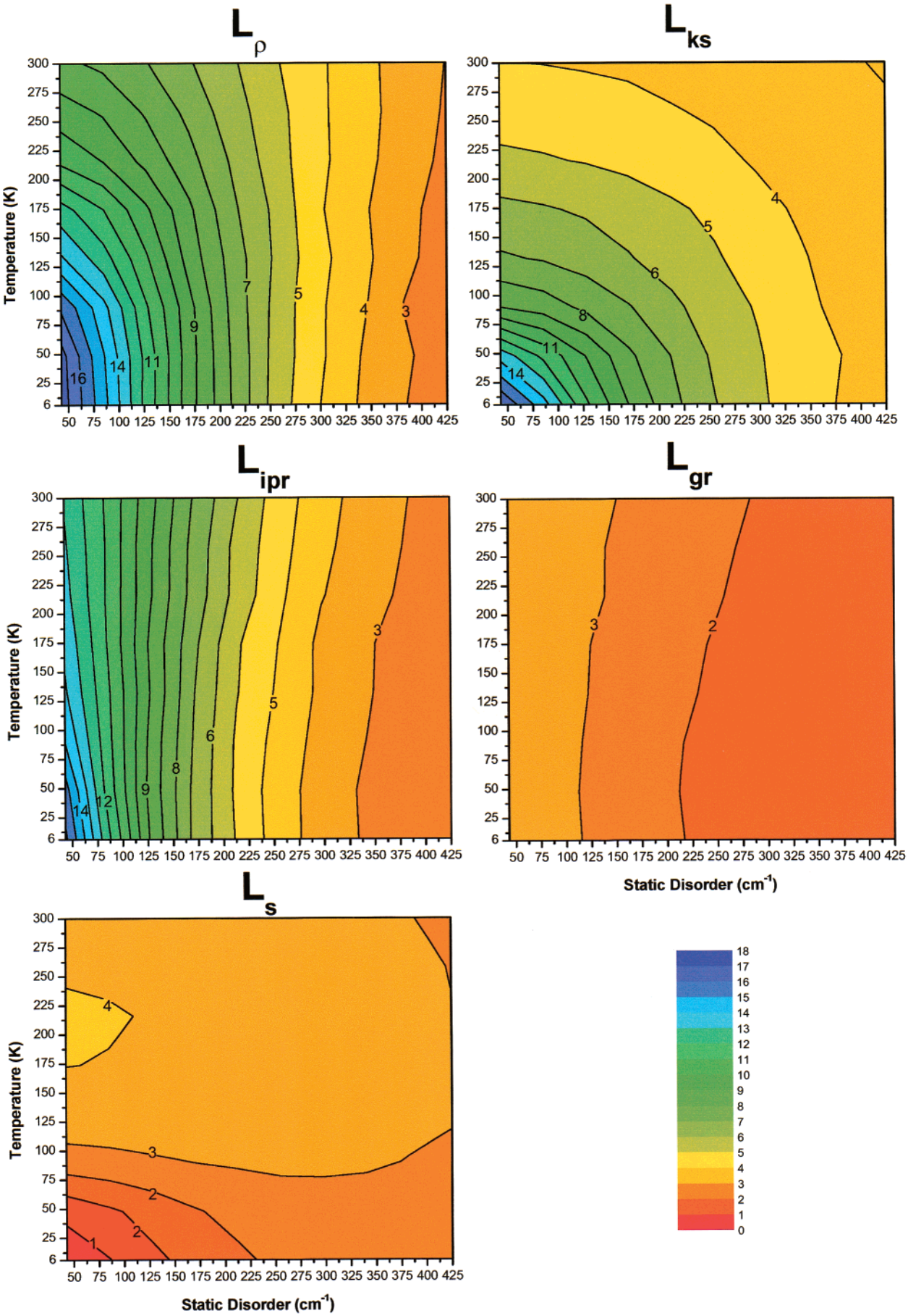

Figure 3. Panels displaying the result from the corresponding definitions of L_d given in section III. In all cases, the exciton was calculated in the thermalized state.

homogeneous and inhomogeneous broadening[14] is based on the separation of the bath fluctuation time scales. We find that the parameters used here are within the ranges used in the literature. We point out that at higher temperatures the borderline between homogeneous and inhomogeneous parts of the spectrum is not very clear cut and one needs to consider the relevant time scales of the experimental observables which are used in the analyzes. Rigorous treatment of the temperature dependence of spectra goes beyond the scope of the current article, where we have included the temperature via the Redfield relaxation matrix.

The characteristics of the second excited transition ($S_1 \rightarrow S_2$) are less known. On the basis of ref 61, we have used an energetic offset (Δ) between the ($S_1 \rightarrow S_2$) and the ($S_0 \rightarrow S_1$) transitions of $\sim$500 cm^{-1} and further assumed that the respective transition dipoles are parallel and the ratio $\kappa = \mu^{(1\rightarrow 2)}/\mu^{(0\rightarrow 1)}$ is 0.6. All parameters were further verified by comparing calculated and measured transient absorption spectra (see below).

We consider the pulse duration to be short compared to the nuclear dynamics, but long compared to the electronic dephasing time scale. The snapshot doorway wave packet[14] was convoluted with the Gaussian spectral profile of the excitation pulse,

$$I(\omega_1 - \bar{\omega}_1) = \frac{1}{\sigma_1\sqrt{2\pi}} \exp(-(\omega_1 - \bar{\omega}_1)^2/2\sigma_1^2) \quad (4.2)$$

where $\bar{\omega}_1$ is the pulse central frequency with a variance of 151 cm^{-1} for the pump pulse (which corresponds to a Gaussian pulse with a fwhm duration of $\sim$40 fs).

In ref 26 the reorganization energy (λ) of the B850 aggregate was estimated using the three pulse photon echo peak shift (3PEPS) experiment to be about 40 cm^{-1}. In order for the Redfield theory to yield relaxation and dephasing rates comparable with experiment, we used a reorganization energy of 130 cm^{-1}. This difference is most likely due to our bath model, consisting of a single overdamped Brownian oscillator per chromophore. In addition, the aggregate reorganization energy reported in ref 26 is different from the molecular reorganization energy used here. We assumed an inverse nuclear relaxation time (Λ) of 1300 cm^{-1}. These parameters satisfy the necessary condition, $\Lambda/\lambda \gg 1$ required for the applicability of the Redfield equations.

The parameters above will now be used to analyze the exciton coherence size in LH2. The various measures of L_d are very similar in the two limiting cases, i.e., $L_d \sim 18$ for zero temperature without disorder and $\sim$1 in the other extreme limit. However, for the generalized inverse participation ratio (L_{gr}) and the superradiance factor (L_s) the analysis is more subtle. For the former definition, one needs to let $\Gamma \rightarrow 0$ in order for L_{gr} to approach 18 (doing so reduces the definition to that of the ordinary inverse participation ratio). The superradiance factor (L_s) for a ringlike structure goes to zero at low temperature without disorder (see below).

Figure 3 displays the dependence of L_d on temperature and disorder for the various different definitions. At room temperature, the thermalized Kühn−Sundström length, L_{ks}, is about 4 BChl pigments, in good agreement with previously reported results for a static disorder with a Gaussian profile and a variance of about 210 cm^{-1}.[23] As can be seen from the figure, this definition of L_d depends quite strongly on both temperature and inhomogeneous broadening. L_ρ results in a qualitatively similar behavior to L_{ks}, but it decreases much more slowly with increasing temperature and disorder. A well-defined value of L_ρ can be calculated under all conditions, even when the coherence between exciton levels is large. At room temperature in the thermalized limit L_ρ is about 6 BChl pigments, slightly larger than L_{ks}. L_{ipr}, and L_{gr}, both show a very weak temperature dependence but a strong dependence on disorder. A reasonable static disorder of 250 cm^{-1} at room temperature results in $L_{ipr} \sim 4-5$ BChl molecules, whereas the generalized inverse participation ratio (L_{gr}) gives around 2 pigments. In addition, L_{gr} has a strong dependence on the exciton dephasing rate Γ, which causes a decrease of the delocalization length at all temperatures and disorder realizations.

The superradiance factor (L_s) is displayed in Figure 3 as well. L_s decreases as the temperature and disorder is decreased, in contrast to the behavior of the delocalization lengths discussed above. This behavior reflects the specific geometry of the emitting dipoles included in the definition of L_s (eq 2.8). Since the lowest exciton state is optically forbidden (weakly allowed when disorder is included) for the ringlike symmetry of B850, L_s will decrease at low temperatures when this state becomes highly populated. L_s is estimated to be $\sim$3 at room temperature for 250 cm^{-1} and as the temperature is decreased L_s decreases slowly to roughly 2 at 6 K. Superradiance of B850 was measured by Monshouwer et al. in the temperature range from 6 to 300 K;[18] the superradiance factor was found to be $\sim$3−4 BChls in this temperature range. With the same parameters used to fit the transient absorption spectrum ($\sigma_{inh} = 250$ cm^{-1}, $\Gamma = 75$ cm^{-1}) our calculations result in a very similar behavior of L_s, i.e., $L_s \sim 2.5$ at low temperature (<77 K) and $L_s \sim 3.2$ at 300 K. The superradiance measurements of course yield the thermalized value of the L_s, since this is a time-integrated technique.

To study the temporal evolution of the delocalization length, we fixed the disorder at 210 cm^{-1} and calculated L_d for a series of time delays at 300 K (see Figure 4, panel A), using the three definitions that provide a time dependence. L_d is quite large at short times ($\sim$5−13) and decreases rapidly to $\sim$4−6 sites. Note, however, that L_{ks} at early times is most likely underestimated due to the difficulty in determining the fwhm of the distribution when the coherence between exciton levels is large (see previous section). The calculations show that the exciton dephasing is completed in a few hundred femtoseconds. L_ρ has a slower decay than the other two definitions of L_d, due to the slow population redistribution predicted in this case, also seen in the time-dependent DM plot (panel B).

The localization process can be qualitatively described in a few steps. At time zero, L_d is determined by static properties such as the inhomogeneous broadening and the extent of the coherence between exciton levels created by the pulse. The decrease that takes place at later times is caused by the exciton−phonon interaction. The rapid initial decay seen in panel A can be understood by studying panels B, C, and D, which show the time-dependent EDM elements using the same parameters as in panel A. The rapid decrease in panel A can be assigned mainly to the destruction of the initially prepared coherence between the exciton levels and the initial fast inter exciton level relaxation. The dynamics above $\sim$250 fs reflect the slower part of the population relaxation. The final thermalized size of L_d depends on the combination of the different static parameters such as temperature, disorder, and exciton dephasing.

Time-resolved transient absorption spectra, measured at both room temperature and 77 K with $\sim$100 fs pulses,[42] suggest a spectral evolution on a few hundred femtosecond time scale that may be attributed to the processes leading to exciton localization. We have fitted both the linear absorption spectrum (Figure 2) and the transient spectra (Figure 5), using the same parameter values. Comparing the measured and the calculated

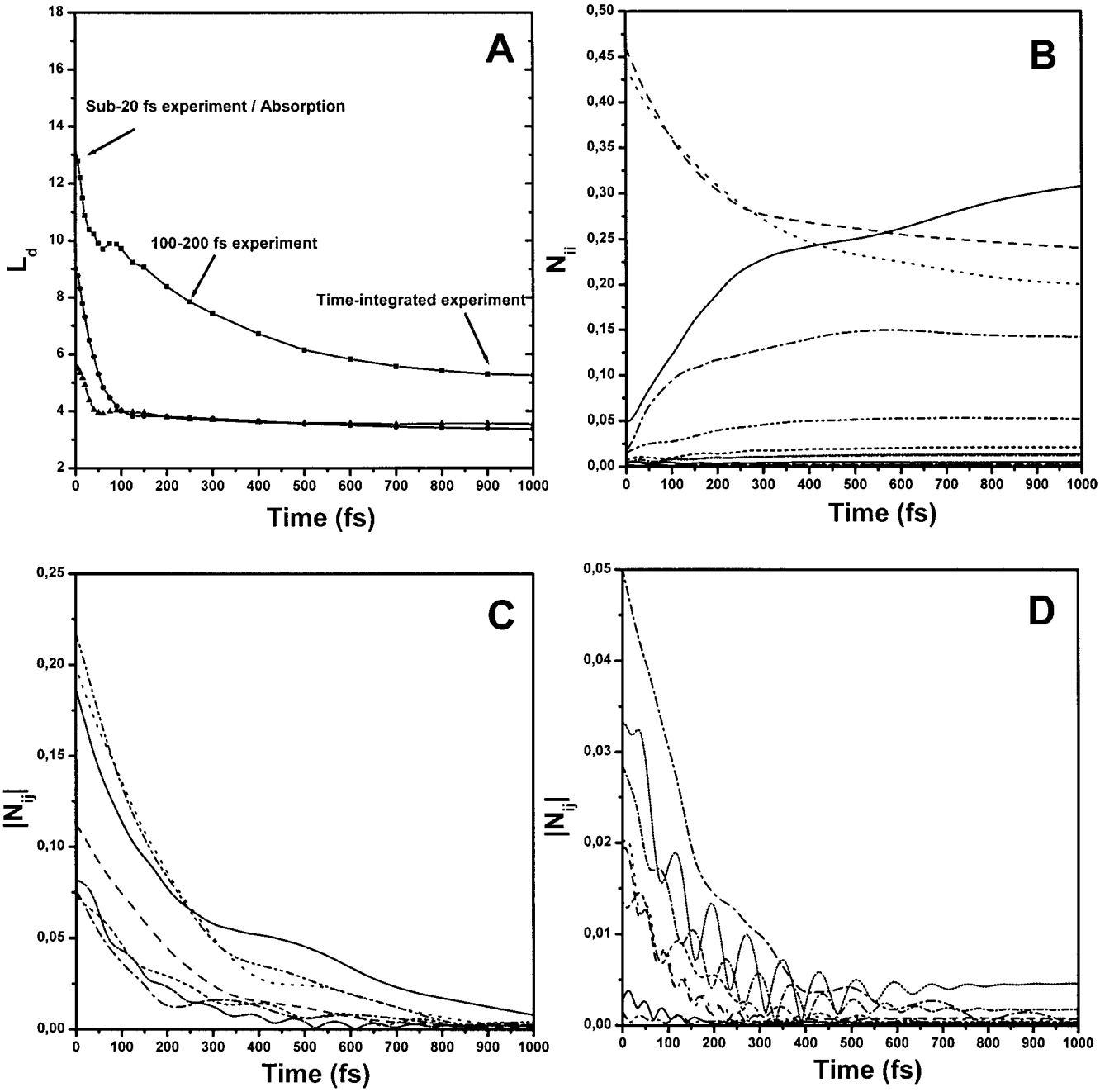

Figure 4. (A) Time evolution of L_ρ (squares), L_s (circles), and L_{ks} (triangles). The inhomogeneous disorder has a variance of 250 cm^{-1} and the spectral density parameters $\lambda = 130$ cm^{-1} and $\Lambda = 1300$ cm^{-1}. (B) The 18 population ($N_{ii}(t)$) elements. (C, D)Amplitude of the largest and the smaller, respectively, off-diagonal coherence elements ($|N_{ij}(t)|$). The time-dependent exciton density matrix elements were calculated at room temperature and with one realization of Gaussian disorder. The pump pulse was tuned to the middle of the one-exciton band, 850 nm.

transient absorption spectra at 200 fs, 500 fs, and 2 ps (Figure 5) strongly suggests that the spectral evolution in fact reflects exciton relaxation and that the B850 exciton evolves from an initially large L_d to a substantially smaller size. This evolution is basically completed in ~1 ps, which is also evident from the time dependence of L_ρ (Figure 4). The faster decay of L_{ks} and L_s is due to the above-mentioned interference problem in the first case and the weak population dependence of the latter. Recent experiments on B850 with high time resolution (~20 fs)[25] also suggest a large exciton size at early time and exciton localization on the time scale of a few hundred femtoseconds.

Finally, in Figure 6 we display the variation of the initial delocalization length with the pump-pulse wavelength between 870 and 810 nm for three different pulse lengths. We point out that we are using the time-domain snapshot limit, which means that we do not calculate the system evolution during the pulses. Various pulse lengths were simulated via different spectral widths of the excitation pulse. A shorter pulse generally creates a larger L_d because of the additional delocalization due to the coherence between exciton levels. The differences between L_d's obtained with 200 fs and 1 ps pulses are negligible since the relatively narrow spectral width of the pulses almost selectively excite only one exciton state and very little inter-exciton coherence is created. L_{ks} does not show any significant dependence on pulse properties, which is partly related to the difficulties with exciton state interference.

Our results imply that the variation of L_d values of B850 reported in the literature results from the use of different

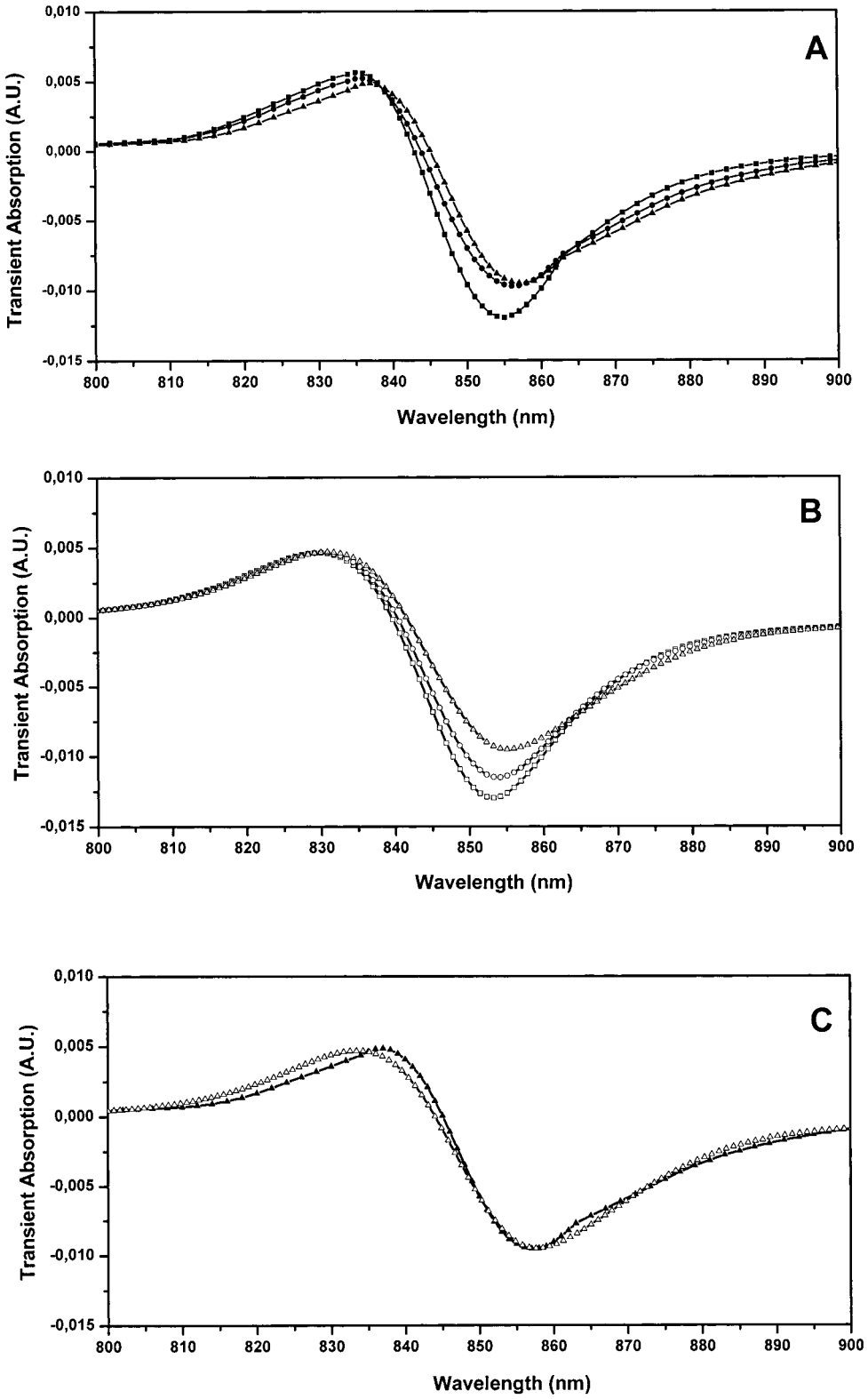

Figure 5. (A) Experimental pump−probe spectra for three different time delays (squares, 200 fs; circles, 500 fs; triangles, 2.0 ps). (B)Simulated spectra for the same time delays as in panel A and with the following parameters: second excited molecular state parameters $\kappa = 0.6$ and $\Delta = 500$ cm^{-1}, respectively; $\Gamma = 75$ cm^{-1}, $\sigma_{inh} = 250$ cm^{-1}. (C) Comparison of the simulated (open triangles) with the experimental (filled triangles) spectra at 2 ps time delay.

techniques and time resolution. Thus, a technique with a time resolution of <25 fs or a technique probing the instantaneous spectral properties should be able to capture the initial size of the exciton wave packet (see also the L_d dynamics illustrated in Figure 4A). On the other hand, a ∼100 fs time-resolved measurement of the kind reported by many authors[30,42] captures some of the evolution but does not provide the initial value of L_d. A steady-state superradiance measurement integrates L_d over the fluorescence lifetime (∼1 ns) of the aggregate and thus provides the thermalized value. Of course, in principle, spontaneous emission could be measured with a time resolution adequate to resolve the localization process. No such measure-

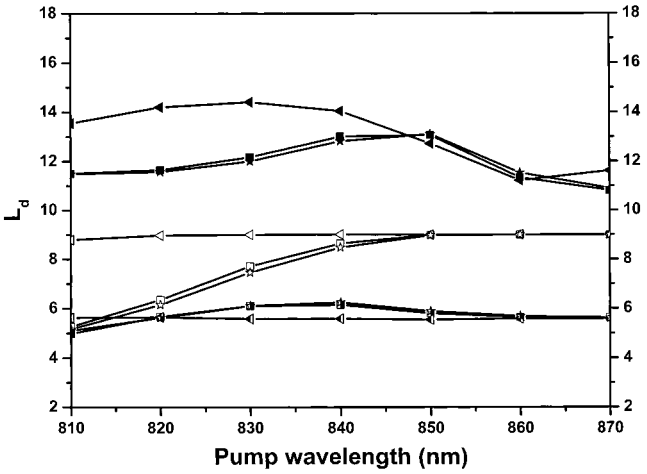

Figure 6. Initial L_d presented for three different pulse durations as a function of wavelength: (filled symbols) L_ρ; (open symbols) L_s; (semifilled symbols) L_{ks}. The different types of symbols correspond to a fwhm of the pulse durations: (triangles) 20 fs; (squares) 200 fs; (stars) 1 ps.

ment has so far been reported. These three different types of experiments are indicated by the arrows in Figure 4, panel A.

V. Conclusions

We have compared the calculated transient absorption spectra to the measured spectra for different time delays. We showed that the spectral dynamics are qualitatively reproduced, both relaxation time scales and spectral evolution. The spectral dynamics correspond to localization of the exciton from an initial substantially delocalized exciton wave packet to a significantly smaller thermalized exciton and occurs on a time scale of a few hundred femtoseconds. We have compared several definitions that provide different estimates of L_d for given disorder parameters and temperature. L_ρ and L_{ks} are constructed using the EDM and sampling over the coherence contributions, but weight these contributions differently, resulting in different dependencies on temperature and disorder. L_ρ is for most parameter values significantly larger than L_{ks}. L_{ipr} and L_{gr} display similar temperature and disorder dependencies, the former is weak while the latter is much more pronounced. Finally, we note that in this paper the exciton−phonon coupling is considered in the weak-coupling limit which introduces transitions between exciton levels (exciton relaxation leading to thermalization) but does not modify the exciton wave functions. The latter would occur in the case of strong electron−phonon interaction, which leads to polaron formation.[42,46,52]

Acknowledgment. We thank Dr. J. L. Herek for critically reading and commenting on the manuscript, Dr. T. Polivka for the experimental data, and Dr. V. Chernyak for enlightening discussions. This work was financially supported by the Crafoord foundation and NFR. S.M. gratefully acknowledges the support of The National Science Foundation and the Petroleum Research Fund administered by the American Chemical Society.

References and Notes

(1) *J-aggregates*; Kobayashi, T., Ed.; World Scientific: Singapore, 1996.
(2) Tretiak, S.; Chernyak, V.; Mukamel, S. *Phys. Rev. Lett* **1996**, *77*, 4656.
(3) Sundström, V.; Pullerits, T.; van Grondelle, R. *J. Chem. Phys. B* **1999**, *103*, 2327.
(4) Tretiak, S.; Chernyak, V.; Mukamel, S. *J. Chem. Phys. B* **1998**, *102*, 3310.
(5) Nakano, M.; Takahata, M.; Fujita, H.; Kiribayashi, S.; Yamaguchi, K. *Chem. Phys. Lett.* **2000**, *323*, 249.
(6) Frenkel, J. I. *Phys. Rev.* **1931**, *37*, 17.
(7) Davydov, A. S. *Theory of Molecular Excitons*; Plenum Press: New York, 1971.
(8) Ziman, J. M. *Models of Disorder*; Cambridge University Press: Cambridge, 1979.
(9) de Bree, P.; Wiersma, D. A. *J. Chem. Phys.* **1979**, *70*, 790.
(10) Pearlstein, R. M.; Hemenger, R. P. *Proc. Natl. Sci. U.S.A.* **1978**, *75*, 4920.
(11) McDermott, G.; Prince, S. M.; Freer, A. A.; Hawthornthwaite-Lawless, A. M.; Papiz, M. Z.; Cogdell, R. G.; Isaacs, N. W. *Nature* **1995**, *374*, 517.
(12) Koepke, J.; Hu, X.; Muenke, C.; Schulten, K.; Michel, H. *Structure* **1996**, *4*, 581.
(13) Pullerits, T.; Hess, S.; Herek, J. L.; Sundström, V. *J. Phys. Chem. B* **1997**, *101*, 10560.
(14) Mukamel, S. *Principles of Nonlinear Optical Spectroscopy*; Oxford University Press: New York, 1995.
(15) Meier, T.; Chernyak, V.; Mukamel, S. *J. Phys. Chem. B* **1997**, *101*, 7332. Zhang, WM.; Meier, T.; Chernyak, V.; Mukamel, S. *J. Chem. Phys.* **1998**, *108*, 7763.
(16) Leegwater, J. A. *J. Chem. Phys.* **1996**, *100*, 14403.
(17) Pullerits, T.; Chachisvilis, M.; Sundström, V. *J. Chem. Phys.* **1996**, *100*, 10787.
(18) Monshouwer, R.; Abrahamsson, M.; van Mourik, F.; van Grondelle, R. *J. Phys. Chem. B* **1997**, *101*, 7241.
(19) Ray, J.; Makri, N. *J. Phys. Chem. A* **1999**, *103*, 9417.
(20) Novoderezkhin, V.; Monshouwer, R.; van Grondelle, R. *J. Chem. Phys. B* **1999**, *103*, 10540.
(21) Meier, T.; Zhao, Y.; Chernyak, V.; Mukamel, S. *J. Chem. Phys.* **1997**, *107*, 3876.
(22) Bakalis, L. D.; Knoester, J. *J. Phys. Chem. B* **1999**, *103*, 6620.
(23) Kühn, O.; Sundström, V. *J. Chem. Phys.* **1997**, *107*, 4154.
(24) Zhao, Y.; Meier, T.; Zhang, W. M.; Chernyak, V.; Mukamel, S. *J. Phys. Chem. B* **1999**, *103*, 3954.
(25) Book, L. D.; Ostafin, A. E.; Ponomarenko, J. R.; Scherer, N. F. *J. Phys. Chem. B* **2000**, *104*, 8295. Book, L. D.; Ostafin, A. E.; Ponomarenko, N.; Norris, J. R.; Scherer, N. F.; Mukamel, S. In *Ultrafast Phenomena XII*; Elsasser, T., Mukamel, S., Murnane M., Scherer, N., Eds.; Springer-Verlag: Berlin, 2000; p 527.
(26) Jimenez, R.; van Mourik, F.; Yu, J. Y.; Fleming, G. R. *J. Phys. Chem. B* **1997**, *101*, 7350.
(27) Kennis, J. T. M.; Streltsov, A. M.; Permentier, H.; Aartsma, T. J.; Amesz, J. *J. Phys. Chem. B* **1997**, *101*, 8369.
(28) Nagarajan, V.; Johnson, E. T.; Williams, J. C.; Parson, W. W. *J. Phys. Chem. B* **1999**, *103*, 2297.
(29) Fidder, H. Thesis, Groningen University 1993.
(30) Chachisvilis, M.; Kühn, O.; Pullerits, T.; Sundström, V. *J. Phys. Chem. B* **1997**, *101*, 7275.
(31) Nagarajan, V.; Alden, R. G.; Williams, J. C.; Parson, W. W. *Proc. Natl. Acad. Sci. U.S.A.* **1996**, *93*, 13774.
(32) Leupold, D.; Stiel, H.; Teuchner, K.; Nowak, F.; Sandner, W.; Ücker, B.; Scheer, H. *Phys. Rev. Lett.* **1996**, *77*, 4675.
(33) Wu, H. M.; Small, G. *J. Chem. Phys.* **1997**, *218*, 225. Wu, H. M.; Ratsep, M.; Lee, I. J.; Cogdell, R. J.; Small, G. *J. Phys. Chem. B* **1997**, *101*, 7654. Wu, H. M.; Small, G. *J. Phys. Chem. B* **1998**, *102*, 888.
(34) Mukamel, S. In *Nonlinear Molecular Optics*; Zyss, J., Ed.; Academic Press: New York, 1994; pp 1−46.
(35) Dubovsky, O.; Mukamel, S. *J. Chem. Phys.* **1991**, *95*, 7828.
(36) Leegwater, J. A.; Mukamel, S. *Phys. Rev. A* **1992**, *46*, 452.
(37) Knoester, J.; Mukamel, S. *Phys. Rep.* **1991**, *205*, 1.
(38) van Oijen, A. M.; Ketelaars, M.; Köhler, J.; Aartsma, T. J.; Schmidt, J. *Science* **1999**, *285*, 400.
(39) Mostovoy, M. V.; Knoester, J. *J. Phys. Chem. B* **2000**, *104*, 12355.
(40) Mukamel, S.; Tretiak, S.; Wagersreiter, T.; Chernyak, V. *Science* **1997**, *277*, 781.
(41) Spano, F. C.; Kuklinski, J. R.; Mukamel, S. *Phys. Rev. Lett.* **1990**, *65*, 211. Spano, F. C.; Kuklinski, J. R.; Mukamel, S. *J. Chem. Phys.* **1991**, *94*, 7534.
(42) Polivka, T.; Pullerits, T.; Herek, J. L.; Sundström, V. *J. Phys. Chem. B* **2000**, *104*, 1088.
(43) Blum, K. *Density Matrix Theory and Applications*; Plenum Press: New York, 1981.
(44) Dahlbom, M.; Minami, T.; Chernyak, V.; Pullerits, T.; Sundström, V.; Mukamel, S. *J. Phys. Chem. B* **2000**, *104*, 3976.
(45) Chernyak, V.; Zhang, W. M.; Mukamel, S. *J. Chem. Phys.* **1998**, *108*, 9587.
(46) Chernyak, V.; Mukamel, S. *J. Chem. Phys.* **1996**, *105*, 4565.
(47) Redfield, A. G. *IBM J. Res.* **1957**, *1*, 19.

(48) Pollard, W. T.; Felts, A. K.; Friesner, R. A. *Adv. Chem. Phys.* **1997**, *93*, 77. Pollard, W. T.; Friesner, R. A. *J. Chem. Phys.* **1994**, *100*, 5054.

(49) Jean, J. M.; Friesner, R. A.; Fleming, G. R. *J. Chem. Phys.* **1992**, *96*, 5827.

(50) Mukamel, S.; Ciordas-Ciurdariu, C.; Khidekel, V. *IEEE* **1996**, *32*, 1278.

(51) Mukamel, S. *J. Chem. Phys.* **1997**, *107*, 4165.

(52) Feynman, R. P. *Statistical Mechanics*; Perseus Books: Reading, MA, 1998.

(53) Chernyak, V.; Meier, T.; Tsiper, E.; Mukamel, S. *J. Phys. Chem. B* **1999**, *103*, 10294.

(54) Kennis, J. T. M.; Aartsma, T. J.; Amesz, J. *Biochim. Biophys. Acta* **1994**, *188*, 278.

(55) Owen, G. M.; Hoff, A. J.; Jones, M. R. *J. Chem. Phys. B* **1997**, *101*, 7197.

(56) Knox, R. S.; Gülen, D. *Photochem. Photobiol.* **1993**, *57*, 40.

(57) Fyodorov, Y. V.; Mirlin, A. D. *Phys. Rev. B* **1995**, *51*, 13403.

(58) Hall, M. J. W. *Phys. Rev. A* **1999**, *59*, 2602.

(59) Plerou, V.; Gopikrishan, P.; Rosenow, B.; Nunes Amaral, L. A.; Stanley, H. E. *Phys. Rev. Lett.* **1999**, *83*, 1471.

(60) The function I_2 is in parts of the literature referred to as the inverse participation ratio, but here we use that designation for I_2^{-1}.

(61) Martinsson, P.; Sundström, V.; Åkesson, E. *FEBS* **2000**, *465*, 107. Martinsson, P.; Thesis, Lund University, **1999**.